

RESEARCH

Open Access



# Age, environment, object recognition and morphological diversity of GFAP-immunolabeled astrocytes

Daniel Guerreiro Diniz<sup>1,3</sup>, Marcus Augusto de Oliveira<sup>1</sup>, Camila Mendes de Lima<sup>1</sup>, César Augusto Raiol Fôro<sup>1</sup>, Marcia Consentino Kronka Sosthenes<sup>1</sup>, João Bento-Torres<sup>1</sup>, Pedro Fernando da Costa Vasconcelos<sup>2</sup>, Daniel Clive Anthony<sup>3</sup> and Cristovam Wanderley Picanço Diniz<sup>1,3\*</sup>

## Abstract

**Background:** Few studies have explored the glial response to a standard environment and how the response may be associated with age-related cognitive decline in learning and memory. Here we investigated aging and environmental influences on hippocampal-dependent tasks and on the morphology of an unbiased selected population of astrocytes from the molecular layer of dentate gyrus, which is the main target of perforant pathway.

**Results:** Six and twenty-month-old female, albino Swiss mice were housed, from weaning, in a standard or enriched environment, including running wheels for exercise and tested for object recognition and contextual memories. Young adult and aged subjects, independent of environment, were able to distinguish familiar from novel objects. All experimental groups, except aged mice from standard environment, distinguish stationary from displaced objects. Young adult but not aged mice, independent of environment, were able to distinguish older from recent objects. Only young mice from an enriched environment were able to distinguish novel from familiar contexts. Unbiased selected astrocytes from the molecular layer of the dentate gyrus were reconstructed in three-dimensions and classified using hierarchical cluster analysis of bimodal or multimodal morphological features. We found two morphological phenotypes of astrocytes and we designated type I the astrocytes that exhibited significantly higher values of morphological complexity as compared with type II. Complexity = [Sum of the terminal orders + Number of terminals] × [Total branch length/Number of primary branches]. On average, type I morphological complexity seems to be much more sensitive to age and environmental influences than that of type II. Indeed, aging and environmental impoverishment interact and reduce the morphological complexity of type I astrocytes at a point that they could not be distinguished anymore from type II.

**Conclusions:** We suggest these two types of astrocytes may have different physiological roles and that the detrimental effects of aging on memory in mice from a standard environment may be associated with a reduction of astrocytes morphological diversity.

**Keywords:** Environment, Exercise, Aging, Astrocytes morphology, Dentate gyrus, Memory

\*Correspondence: cwpdiniz@gmail.com

<sup>1</sup> Laboratório de Investigações Em Neurodegeneração e Infecção, Instituto de Ciências Biológicas, Universidade Federal do Pará, Hospital Universitário João de Barros Barreto, Rua dos Mundurucus 4487, Guamá, Belém, Pará CEP 66073-000, Brazil

Full list of author information is available at the end of the article

## Background

Epidemiological studies have correlated physical and cognitive inactivity with a greater risk of age-related cognitive decline [1, 2]. In contrast, an active lifestyle may help prevent cognitive impairment in old age [3–5]; for recent reviews see [6–9]. Consistent with this view, the decline in memory that is associated with normal or pathological aging appears to be aggravated after institutionalization [10, 11]. Institutionalization is often associated with a standard-like environment with reduced sensory-motor and cognitive stimulation, social interactions, and physical activity, which contribute to a sedentary lifestyle [4, 5, 10, 12]. Similarly, it has been demonstrated that aged mice and rats, maintained in the standard environment of standard laboratory cages, perform worse in learning and memory tasks than those living in an enriched environment [13–24]. To perform spatial learning and memory tasks, the brain must accentuate the differences between old and new experiences, before coding occurs [25]. For that purpose, medial and lateral perforant pathways transmit to dentate gyrus, spatial and non-spatial information that would be necessary to recognize object placement (Where?), identity (What?) and timing (When?) [25].

Cellular and molecular analyses of these events demonstrate that the beneficial effects of environmental enrichment with voluntary exercise are associated with a variety of neuronal and neuroimmunological changes in both young and aged individuals [23, 26–35]. However, most of the documented changes in cell behavior relate to neuronal populations [36–40].

More recently significant contributions have explored possible roles of astrocytes in physiological and pathological brain aging [41]. Much of these outstanding work was done by Verkhratsky and Rodríguez-Arellano (see [104] for recent review), who showed that aging is associated with complex and region-dependent astrocyte remodeling, that may represent life-long adaptive responses [69] and that astrocytes participate in the morphological remodeling associated with synaptic plasticity [42]. However, astrocyte quantitative morphological studies under combined environmental and aging influences, in particular, is not yet largely explored [43–46].

A recent study showed that long-term potentiation and learning improved in chimeric mice generated by transplanting human astroglial progenitor cells into the fore-brain [47]. In those chimeric mice, large regions of the CNS, including the hippocampus, consisted of mouse neurons (and oligodendrocytes) surrounded by human astrocytes and progenitor cells [48]. Both transplanted and control mice were then subject to a battery of learning and memory tasks and chimeric mice demonstrated

enhanced performance on all tests. Those findings suggested that human astrocytes in particular, might contribute significantly, at least in part, to improved cognition [49, 50]. Morphologically, human astrocytes are larger and structurally more complex than mouse astrocytes [51]. Compared with mouse astrocytes, human astrocytes have soma diameters 2.6  $\mu$ m longer, with tenfold more glial fibrillary acid protein (GFAP)-positive processes and fourfold faster calcium waves [52].

Taken together, these findings raise important questions related to the morphology of astrocytes and cognition. For example, is the performance of animals with more complex immunolabeled astrocytes in the dentate gyrus, associated with better performances in object-identity tasks?

Thus, in the present report we described possible associations between environmental and age changes with alterations in the morphological complexity of GFAP immunolabeled astrocytes of the molecular layer of dentate gyrus, the main target of perforant pathway in mammals [53], and searched for potential associations between higher performances in the object recognition tests and higher morphological complexity of astrocytes.

## Methods

### Animals and experimental groups

More detailed experimental procedures have been previously described elsewhere [13]. Seventy-one Swiss female adult (6 months old—6 M) and aged (20 months old—20 M) mice were housed from 21st postnatal day either in enriched conditions ( $n = 42$ ) or in standard conditions ( $n = 29$ ). They remained as such until the sacrifice in each time window. These formed four experimental groups: enriched environment, young adults (EY,  $n = 12$ ); standard environment, young adults (IY,  $n = 13$ ); enriched environment, aged adults (EA,  $n = 30$ ); and standard environment, aged adults (IA,  $n = 16$ ). Enriched conditions comprised 2-level wire cages ( $100 \times 50 \times 100$  cm) equipped with ropes, rod bridges, tunnels, running wheels, and toys. Toys were made of different forms of plastic, wood and metal of different colors, and were changed periodically. Each enriched cage housed 12–15 young and aged mice from housed from weaning in enriched conditions (EC,  $n = 27$ ) or impoverished conditions (IC,  $n = 29$ ). Water and food were delivered to the top and bottom levels, respectively. This obliged mouse to move from one compartment to another for drinking and eating. Standard conditions comprised plastic cages ( $32 \times 39 \times 100$  cm) without equipment or toys. Each standard cage housed 12–13 young and aged mice. All mice had free access to water and food. In addition, 12-h dark and light cycles were maintained. Behavioral tests were administered during the light cycle.

## Object recognition tasks

### Behavioral procedures

Current learning analyses do not use dynamic estimation methods and require many trials across many animals to assess significant differences in learning. Moreover, they provide no consensus on how best to identify when learning was occurred [54]. In the present work we used single trial tests to assess object recognition [55].

The apparatus for the single trial object recognition test consisted of an open box (30 × 30 × 40 cm) made of painted white wood. The floor was painted with lines to form nine squares (10 × 10 cm) and the luminance at the center of the cage floor was 2.4 cd/m<sup>2</sup>. Detailed protocols and reasons for test choices were discussed elsewhere [55, 56]; see also [57, 58] for reviews). In brief, behavioral essays were performed over 17 days: 7 days for handling, 3 days for open field habituation, 2 days for object habituation, and 5 days for testing: 1 day for each test. *Handling*: each day mice were placed in the center of the arena for 1 min and then removed to their cages. *Open field habituation*: each day mice were placed in the arena, free of objects, for 5 min to explore the open field. *Object habituation*: each day mice were exposed to two identical objects placed at the corners of the arena for 5 min, three times, with 50 min in between. These objects were not used on the test days. *Testing*: one-trial recognition tests were administered on five consecutive days: the object identity test, the object placement test, the object timing test, the context test, and the episodic-like memory test.

In order to minimize the influence of natural preferences for particular objects or materials, we chose objects of the same material but different geometries that could be easily discriminated and had similar possibilities for interaction [55]. All objects were plastic with different shapes, heights, and colors. Before each mouse entered the arena, the box and objects were cleaned with 75 % ethanol to minimize distinguishing olfactory cues.

*One-trial object identity recognition* consisted of a 5-min sample trial, during which subjects explored two identical objects in a familiar arena, followed by a 50-min intermission and then a second 5-min test trial, in which a “novel” object was presented together with one “familiar” object already explored during the sample trial. Objects differed in form, dimensions, color, and texture and had no ethological significance for mice.

*One-trial object placement recognition* followed the same procedure as above, except in the test trial, one of the two identical objects was shifted to a novel location (“displaced” object).

*One-trial object timing recognition* consisted of three trials: two 5-min sample trials during which subjects explored two different object pairs; each trial was followed by a 50-min intermission; then one 5-min test trial

in which one “former” and one “recent” object were presented together.

*One-trial object context recognition* also consisted of three trials: two 5-min sample trials and one 5-min test trial, each separated by 50 min intermissions. During the sample trials objects were presented in different ambient contexts. In the first sample trial two identical objects were presented under a bright light with extra-arena visual cues. In the second sample trial two different identical objects were presented under a dim light with different extra-arena visual cues. In the test trial two objects, one from each sample trial, were presented simultaneously in the bright light context [59].

All tests were video recorded by web cam and most images were analyzed with a computer program to score the time spent interacting with objects and the water maze performances (ANYMAZE tracking system, Stöeltz). Computer analysis was done off-line. Exploration of an object was assumed when a mouse approached an object, the head was directed towards it, and the head was placed within 0–3 cm from the object. This definition required that each object be fixed to the apparatus floor, thus we chose heavy objects for interaction. Diagrams of the object recognition memory tests used in the present report are shown in Fig. 2 and the performance on each test is defined as the percentage of time spent exploring one object. To account for individual variability in exploratory activity, the time spent with each object was normalized by the total exploration time for each individual.

### Statistical analysis

Detailed statistical procedures for object recognition tests were described elsewhere [60]. Normality of the data distribution was tested and outliers were rarely removed from samples based on standard deviations. In brief, for object recognition tests, the basic measure obtained from video-images was the time a mouse spent exploring each object during the test trial, and scores were determined for recognition of identity (novel vs familiar), placement (displaced vs stationary), timing (recent vs former) and contextual (new context vs familiar context) memories. The data were analyzed by parametric statistics and the two-tailed t test for dependent groups was used to detect significant differences. The performance was the time of exploration for each object expressed as a proportion (percentage) of the total time of exploration, and possible significant differences were also detected with the two-tailed t test for dependent groups [59]. In all statistical tests the threshold for significance was set at  $p < 0.05$ .

### Perfusion and histological procedures

At the end of behavioral tests, 5–9 animals from each experimental group were weighed and killed with an

overdose of ketamine (100 mg/kg) and xylazine (10 mg/kg) (Konig Laboratories). They were then perfused transcardially with heparinized saline for 10 min, followed by an aldehyde fixative (4 % paraformaldehyde in 0.1 M phosphate buffer, pH 7.2–7.4) for 30 min. All other chemicals were purchased from Sigma (São Paulo, Brazil). After perfusion and craniotomy, the brains were removed and cut on a vibratome (70  $\mu$ m thickness). One of each five sections was used to detect GFAP by free-floating immunohistochemistry. Free-floating sections were rinsed once in 0.1 M phosphate buffer, transferred to 0.2 M boric acid pH 9.0, heated to 65–70 °C for 1 h, and then washed 3  $\times$  5 min in 5 % PBST. The sections were incubated under constant gentle shaking in a 1 % hydrogen peroxide solution in methanol for 10 min, then rinsed 2  $\times$  2 min in 0.1 M PBS. The sections were blocked with immunoglobulin for 1 h using the Mouse-on-Mouse Immunodetection kit (M.O.M. kit, Vector Laboratories, USA) according to the manufacturer's instructions. Blocking was followed by washing for 3  $\times$  2 min in PBS. Sections were incubated in a working solution of protein concentrate for 5 min, then incubated with monoclonal mouse anti-GFAP primary antibody (MAB360, CHEMICON Int., USA), diluted in protein concentrate solution (M.O.M. kit), at 4 °C for 3 days with continuous, gentle agitation. Next, the sections were washed 3  $\times$  2 min in PBS and incubated for 20 h with biotinylated horse anti-mouse secondary antibody (M.O.M. kit), diluted 1:100 in PBS. After washing 3  $\times$  2 min in PBS, sections were transferred to an avidin–biotin–peroxidase complex solution (ABC, Vector Laboratories, USA, 1:200) for 1.5 h, washed 3  $\times$  2 min in 0.1 M PBS, and processed with the glucose oxidase-DAB-nickel method and peroxidase histochemistry [61].

The reaction was interrupted after fine astrocytic branches were detected under the microscope. Sections were rinsed 4  $\times$  5 min in 0.1 M PBS, mounted on gelatinized slides, dehydrated in alcohol and xylene, and coverslipped with Enthelan (Merck). Five animals from each group with complete GFAP immunohistochemistry slide collections that contained conspicuous morphological details of astrocytes were used for 3-D reconstruction and morphometric analysis.

### 3-D astrocyte reconstruction and quantitative morphology

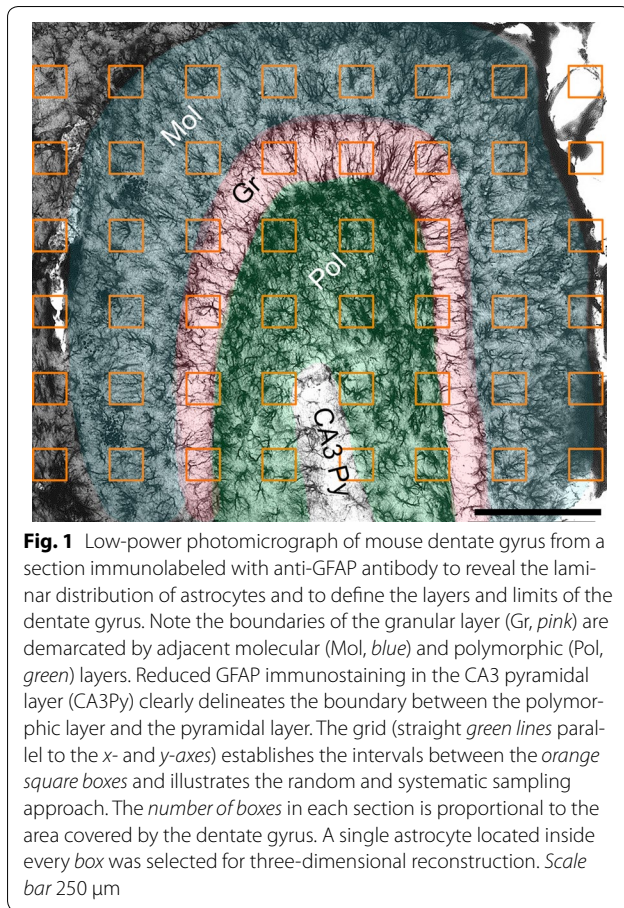
We selected five brains from each experimental group for GFAP immunolabeling and 3-D reconstruction. To analyze brain sections, we used a NIKON Eclipse 80i microscope (Nikon, Japan) equipped with a motorized stage (MAC6000, Ludl Electronic Products, Hawthorne, NY, USA). Astrocytes from the layer of interest were analyzed under oil immersion, with a high-resolution,

100  $\times$  oil immersion, plan fluoride objective (Nikon, NA 1.3, DF = 0.19  $\mu$ m). Images were acquired with NeuroLucida and analyzed with NeuroLucida explorer software (MBF Bioscience Inc., Frederick, MD, USA). Although shrinkage in the z-axis is not a linear event, we corrected the shrinkage in the z-axis, based on previous evidence of 75 % shrinkage [62]. Without correction, this shrinkage would significantly distort the length measurements along this axis. Only cells with processes that were unequivocally complete were included for 3-D analysis; cells were discarded when branches appeared artificially cut or not fully immunolabeled. Terminal branches were typically thin.

### Morphometric analysis and statistics

To accomplish the analysis, we used 20 animals, five from each experimental group (IY, n = 5; EY, n = 5; EA, n = 5; IA, n = 5). From these four groups, we digitally reconstructed 309 astrocytes in three-dimensions from the molecular layer (EY = 79, IY = 75, EA = 76, IA = 79) of the dentate gyrus. Astrocytes for 3-D reconstructions were selected in an unbiased, randomized, and systematic way (Fig. 1). We used architectonic differences in the neuropil region, readily visible in immunolabeled sections, to define the limits of the dentate gyrus layers of the hippocampus. Systematic and random samples were taken from a series of sections containing dorsal and ventral dentate gyrus to guarantee that all regions had the same probability of being included among the analyzed samples. Each box inside the outlined dentate gyrus layers indicates a site from which we selected a single astrocyte for 3-D reconstruction (Fig. 1).

We first investigated the presence of morphological features shared by the astrocytes observed in each layer of interest in our sample, inside each experimental group. We selected all morphometric quantitative variables with multimodality indices (MMI) higher than 0.55, to an initial cluster analysis (Ward's hierarchical clustering method), which included all animals from each group. To estimate the multimodality index (MI) based on skewness and kurtosis of our sample for each morphometric variable as previously defined elsewhere:  $MI = [M3^2 + 1] / [M4 + 3(n - 1)^2 / (n - 2)(n - 3)]$ , where M3 is skewness and M4 is kurtosis and n is sample size [63, 64]. Kurtosis and skewness describe the shape of the data distribution and enable to distinguish between unimodal, bimodal or multimodal curves. Multimodal data sets are essential for separating a population of cells into cell types [63]. The multimodal index of each variable was estimate based on the measurements of 30 morphometric features of astrocytes, 10 related to the soma and 20 to the branches, as follows: 1. Soma area ( $\mu$ m<sup>2</sup>); 2. Soma perimeter; 3. Feret



minimum diameter; 4. Feret Mouse maximum diameter (maximum diameter in a shape); 5. Compactness; 6. Form factor; 7. Solidity; 8. Roundness; 9. Aspect ratio; 10. Convexity; 11. Branch length ( $\mu\text{m}$ ); 12. Total tree length ( $\mu\text{m}$ ); 13. Surface area ( $\mu\text{m}^2$ ); 14. Branch volume ( $\mu\text{m}^3$ ); 15. Segments/mm; 16. Tortuosity; 17. Fractal dimensions (k-dim); 18. Base diameter of the primary branch ( $\mu\text{m}$ ); 19. Total number of segments; 20. Number of varicosities; 21. Planar angle; 22. Number of trees; 23. Complexity; 24. Convex hull volume; 25. Convex hull surface; 26. Convex hull area; 27. Convex hull perimeter; 28. Vertex Va; 29. Vertex Vb; 30. Vertex Vc. Table 1 contains descriptions of all morphometric variables used.

We found that a few microglial morphological features showed a multimodality index greater than 0.55 and this index value indicates that the distribution is at least bimodal and may be multimodal, and these particular features were selected for cluster analysis as previously described [63]. We used the Ward's method with standardized variables, square Euclidian distances and a tree diagram (dendrogram) to illustrate the classification

generated by cluster analysis. From hierarchical cluster analysis we categorized astrocytes into two groups designated types I and II.

We applied this multivariate statistical procedure to our sample of astrocytes in order to search for potential astroglial morphological classes inside of each experimental group. The classification of astrocytes suggested by cluster analysis was assessed using a forward stepwise discriminant function analysis performed with Statistica 12.0 (Statsoft, Tulsa, OK). Discriminant function analysis was used to determine which variables discriminate between two or more naturally occurring groups. The purpose of this procedure is to determine whether the groups differ with regard to the mean of a variable, and then to use that variable to predict group membership. In the present study, we used this software to perform comparisons between matrices of total variances and co-variances. These matrices were compared using multivariate F tests to determine whether there were any significant between-group differences (with regard to all variables). In the step-forward discriminant function analysis, the program builds a model of discrimination step-by-step. In this model, at each step, all variables are reviewed and evaluated to determine which variable contributes most to the discrimination between groups. We applied this procedure to determine morphometric variables that provided the best separation between the astroglial classes suggested by the cluster analysis. In addition, we calculated the arithmetic mean and standard deviation for the variables chosen as the best predictors for the astroglial groups. Parametric statistical analyses with t tests were applied to compare groups of astrocytes inside each experimental group and to detect possible morphological differences between average astrocytes from molecular layer of each experimental group. In the selected sections, the margins of the polymorphic, granular, and molecular layers were clearly distinguished with Nissl counterstaining.

All astrocytes from each layer of interest were measured multiple times, and dedicated software (NeuroLucida explorer, MicroBright Field Inc.) was used to process data obtained with NeuroLucida.

## Results

### Behavioral outcomes

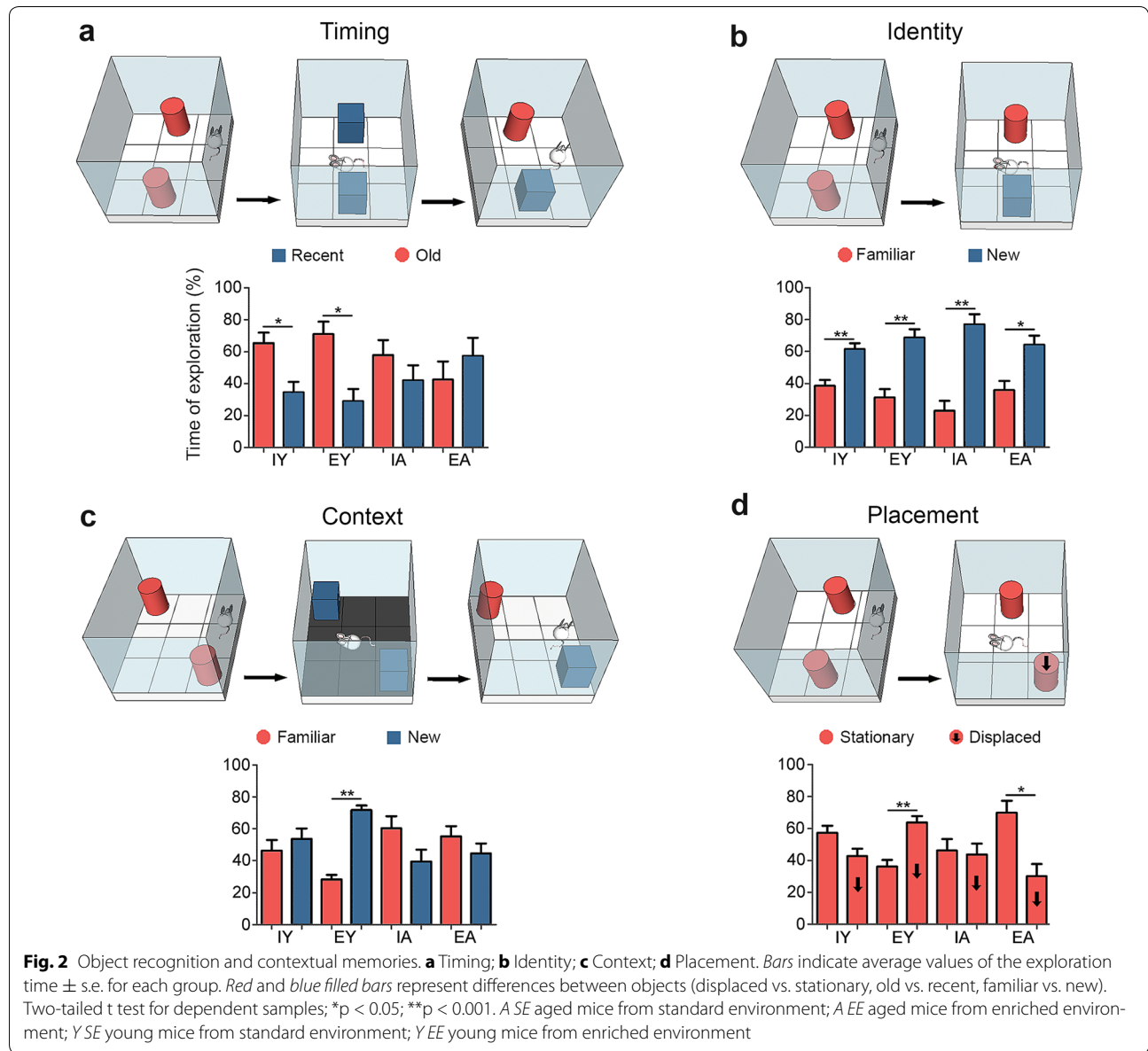
Results of the object recognition tests are shown in Fig. 2. All experimental groups were able to distinguish familiar from new objects (identity—What?). All other tasks were significantly influenced by age, environment, or both as follow:

**Table 1 Morphometric features definitions**

<i>Branched structure analysis</i>	
Segment	Any portion of microglial branched structure with endings that are either nodes or terminations with no intermediate nodes
Segments/mm	Number of segments/total length of the segments expressed in millimeters
No of trees	Number of trees in the astrocytes
Total no of segments	Refer to the total number of segments in the tree
Branch length	Total length of the line segments used to trace the branch of interest.
Total branch length	Total length for all branches in the tree Mean = [length]/[number of branches]
Tortuosity	=[Actual length of the segment]/[distance between the endpoints of the segment]. The smallest value is 1; this represents a straight segment. Tortuosity allows segments of different lengths to be compared in terms of the complexity of the paths they take
Surface area	Computed by modeling each branch as a frustum (truncated right circular cone)
Tree surface area	
Branch volume	Computed by modeling each piece of each branch as a frustum.
Total branch volume	Total volume for all branches in the tree
Base diameter of primary branch	Diameter at the start of the 1st segment
Planar Angle	Computed based on the endpoints of the segments. It refers to the change in direction of a segment relative to the previous segment
Fractal dimension	The "k-dim" of the fractal analysis, describes how the structure of interest fills space. Significant statistical differences in k-dim suggest morphological dissimilarities
Convex hull-perimeter	Convex hull measures the size of the branching field by interpreting a branched structure as a solid object controlling a given amount of physical space. The amount of physical space is defined in terms of convex-hull volume, surface area, area, and or perimeter
Vertex analysis	Describes the overall structure of a branched object based on topological and metrical properties. Root (or origin) point: For neurons, microglia or astrocytes, the origin is the point at which the structure is attached to the soma. Main types of vertices: $V_d$ (bifurcation) or $V_t$ (trifurcation): Nodal (or branching) points. $V_p$ : Terminal (or pendant) vertices. $V_a$ : primary vertices connecting 2 pendant vertices; $V_b$ : secondary vertices connecting 1 pendant vertex ( $V_p$ ) to 1 bifurcation ( $V_d$ ) or 1 trifurcation ( $V_t$ ); $V_c$ : tertiary vertices connecting either 2 bifurcations ( $V_d$ ), 2 trifurcations ( $V_t$ ), or 1 bifurcation ( $V_d$ ) and 1 trifurcation ( $V_t$ ). In the present report we measure the number of vertices $V_a$ , $V_b$ and $V_c$
Complexity	Complexity = [sum of the terminal orders + number of terminals] × [total branch length/number of primary branches]
<i>Cell body</i>	
Area	Refers to the 2-dimensional cross-sectional area contained within the boundary of the cell body
Perimeter	Length of the contour representing the cell body
Feret max/min	Largest and smallest dimensions of the cell body as if a caliper was used to measure across the contour. The two measurements are independent of one another and not necessarily at right angles to each other
Aspect ratio	Aspect ratio = [min diameter]/[max diameter] Indicates the degree of flatness of the cell body Range of values is 0–1 A circle has an aspect ratio of 1
Compactness	$\text{Compactness} = \frac{\sqrt{\left(\frac{4}{\pi}\right) \times \text{Area}}}{\text{MaxDiam}}$ The range of values is 0–1 A circle is the most compact shape (compactness = 1)
Convexity	Convexity = [convex perimeter]/[perimeter] A completely convex object does not have indentations, and has a convexity value of 1 (e.g., circles, ellipses, and squares) Concave objects have convexity values less than 1 Contours with low convexity have a large boundary between inside and outside areas
Form factor	$\text{Formfactor} = 4\pi \times \frac{\text{Area}}{\text{perimeter}^2}$ As the contour shape approaches that of a perfect circle, this value approaches a maximum of 1.0 As the contour shape flattens out, this value approaches 0
Roundness	Roundness = [compactness] <sup>2</sup> Use to differentiate objects that have small compactness values

**Table 1 continued**

Solidity	<p>Solidity = [area]/[convex Area]                  The area enclosed by a 'rubber band' stretched around a contour is called the convex area                  Circles, squares, and ellipses have a solidity of 1                  Indentations in the contour take area away from the convex area, decreasing the actual area within the contour</p>
----------	--------------------------------------------------------------------------------------------------------------------------------------------------------------------------------------------------------------------------------------------------------------------------------------------------------------------------------------------------------------------



**One trial object timing recognition**

Young adult mice, independent of environment, were able to distinguish older from recent objects (When?) (Y SE:  $t = 2.38$ ,  $p = 0.0411$ ; Y EE:  $t = 2.72$ ,  $p = 0.0235$ ). In contrast, aged mice independent of environment were unable to make this distinction (A SE:  $t = 0.83$ ,  $p = 0.426$ ; A EE:  $t = 0.66$ ,  $p = 0.526$ ).

**One-trial object identity recognition**

Young adult and aged subjects, independent of environment, were able to distinguish familiar from novel objects. Y SE:  $t = 4.49$ ,  $p = 0.0015$ ; Y EE:  $t = 3.60$ ,  $p = 0.0058$ ; A SE:  $t = 4.30$ ,  $p = 0.0020$ ; A EE:  $t = 2.45$ ,  $p = 0.0364$ .

### One trial object context recognition

Only young mice from an enriched environment were able to distinguish novel from familiar contexts. Y SE:  $t = 0.033$ ,  $p = 0.973$ ; Y EE:  $t = 7.56$ ,  $p < 0.0001$ ; A SE:  $t = 1.39$ ,  $p = 0.201$ ; A EE:  $t = 0.87$ ,  $p = 0.406$ .

### One trial object placement recognition

Aged mice from standard conditions were unable to distinguish stationary from displaced objects (A SE:  $t = 0.274$ ,  $p = 0.789$ ), however young mice, raised in similar conditions were able to do so (Y SE:  $t = 2258$ ,  $p = 0.0503$ ). In contrast, animals from enriched environments, independent of age, were able to distinguish stationary from displaced objects (Where?) with different preferences: young mice spent more time with displaced objects and aged mice with stationary objects (Y EE:  $t = 3.38$ ,  $p = 0.0081$ ; A EE:  $t = 2.62$ ,  $p = 0.0305$ ). Additional file 1: Table S1 shows absolute values of time of exploration on each hippocampal-dependent task for all experimental groups.

### Morphological phenotypes of astrocytes in the molecular layer of dentate gyrus

We used microscopic 3-D reconstructions and an unbiased, systematic, randomized sampling approach to select astrocytes from the molecular layers of the dentate gyrus. Cluster and discriminant analysis illustrate these findings, together with 3-D reconstructions of astrocytes with morphological features close to the “mean astrocyte” of each experimental group. These findings are shown in Figs. 3, 4, 5, 6.

Based on morphometric features and hierarchical cluster analysis using multimodal parameters, we proposed to designate type I and type II as a function of their morphological complexities. As compared to type II, type I was the group of astrocytes with significant higher mean values of complexity. Table 2 summarizes discriminant analysis results and reveals that a few morphological measurements are enough to distinguish Type I from Type II astrocytes in the molecular layer of different experimental groups. Among them, morphological complexity was the morphological feature that contributed most to cluster formation. Complexity is a combination of different morphological features of astrocytes trees. Longer and more ramified astrocytes show higher values of complexity. Based on this parameter we measured the influence of aging and environment on dentate gyrus astrocytes morphology.

Figure 3a represents the hierarchical cluster analysis of the molecular layer astrocytes morphological features from young mice raised in enriched environment. As previously mentioned, this analysis was done using the morphological parameters with MMI >0.55 as

follow: branch volume, aspect ratio, convexity, form factor, complexity, convex hull volume, convex hull surface, convex hull area. Two main clusters of astrocytes were distinguished in the molecular layer of this group and the variables that most contributed to their formation were complexity ( $p < 0.29 \times 10^{-9}$ ) and convex hull volume ( $p < 0.12 \times 10^{-4}$ ). The astrocyte features corresponding to clusters I (Fig. 3b) and II (Fig. 3D) where the presence of significant differences in complexity and convex hull volumes. Figure 3c is a graphic representation of the discriminant analysis to illustrate the distribution of astrocytes in X–Y plot. Note that type I astrocytes dots are more dispersed than type II and the spatial distribution of type I and II dots are quite distinct. Similar analysis was applied to the astrocytes from young adult raised in standard cages (Fig. 4a–d), and to the astrocytes from aged mice raised in enriched (Fig. 5a–d) or in standard cages (not illustrated). Except for the aged mice group from standard environment, showing a single morphological phenotype, all other cases showed two distinct astrocyte morphologies, with notable differences in the mean values of complexity. Indeed, because molecular layer astrocytes from aged mice raised in standard environment were morphologically homogeneous with small Euclidian distances, we could not distinguish type I from type II astrocytes in this group (not illustrated). Surprisingly, in relative terms, the reduction of morphological complexity in both type I and II astrocytes was higher in aged mice maintained in enriched environment than in aged mice from standard environment (Fig. 6). We found no difference between type I and II astrocytes in the molecular layer of aged mice from a standard environment and this was associated with spatial memory impaired performance. In contrast, we still detected significant differences between type I and II astrocytes in aged animals from enriched environment and this was associated with intact spatial memory suggesting that the morphological diversity of astrocytes may be important to maintain spatial memory integrity.

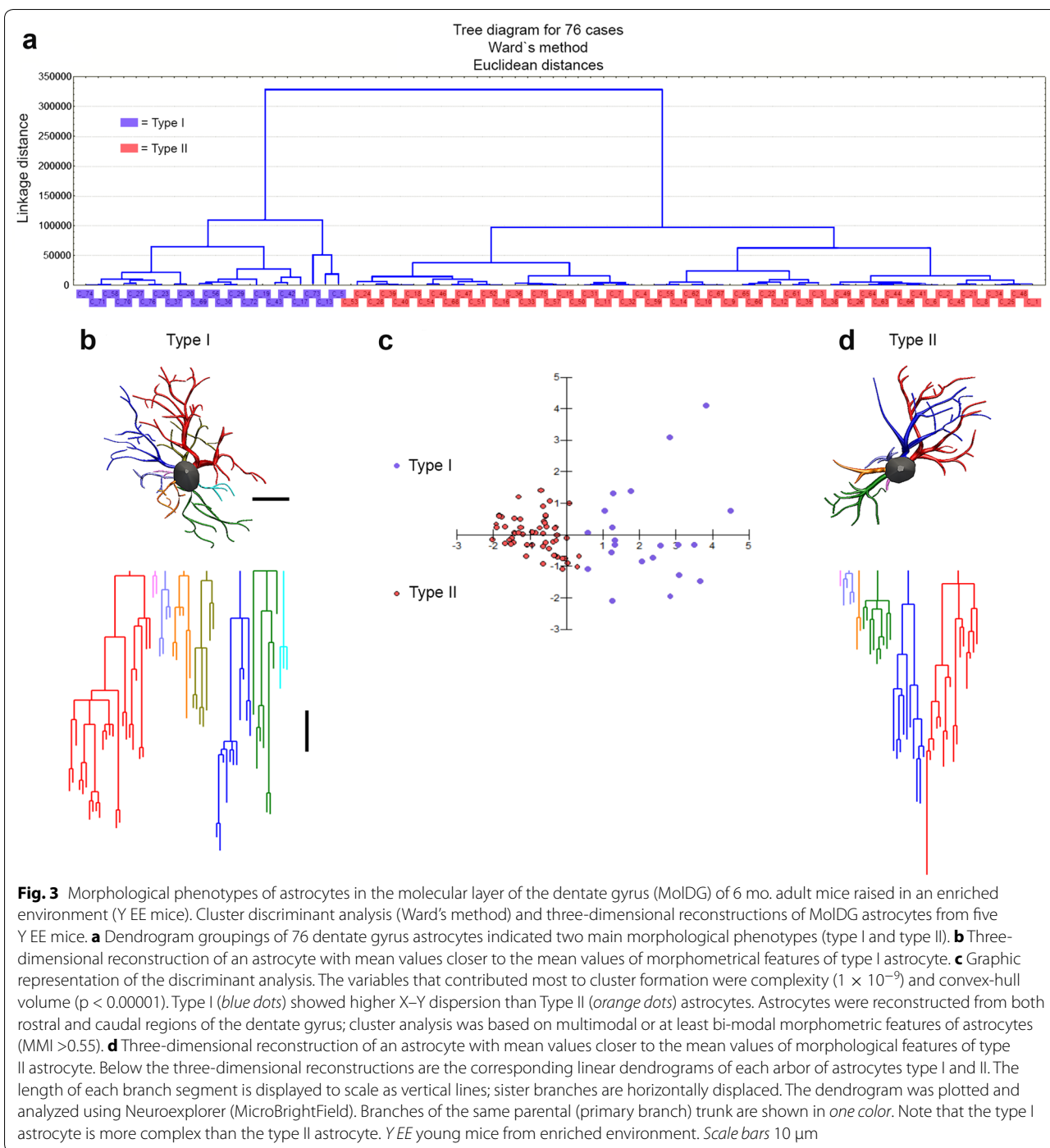
### Influences of environment and age on the morphological complexity of astrocytes in the dentate gyrus

Complexity has been defined previously [65] using the following equation:

$$\text{Complexity} = [\text{Sum of the terminal orders} + \text{Number of terminals}] \times [\text{Total branch length} / \text{Number of primary branches}].$$

See <http://www.mfbioscience.com/help/nx11/Default.htm#Analyses/BranchedStructure/neuronSumm.htm> for details.

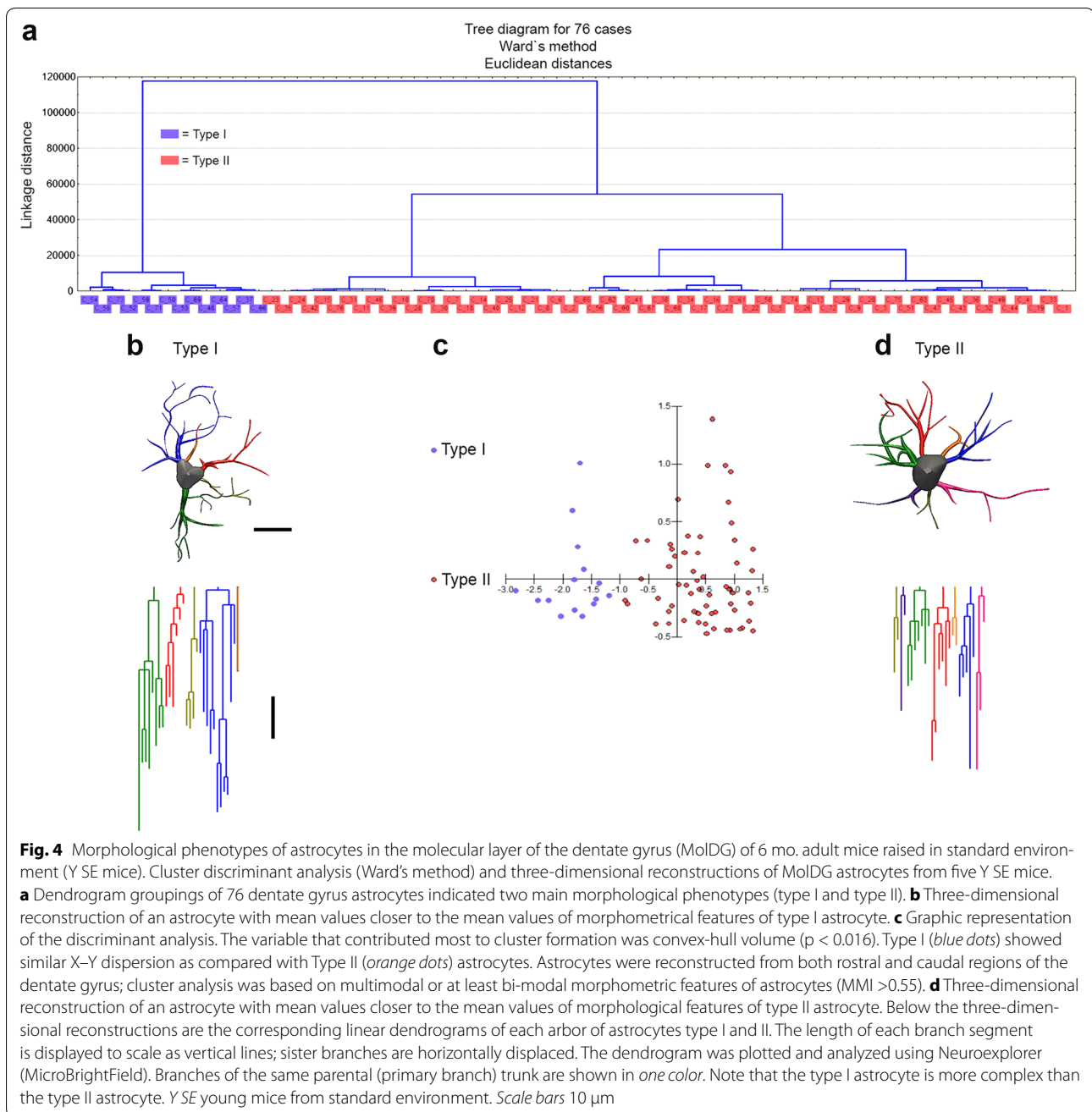
As previously mentioned, more ramified and longer astrocytes are given higher values of complexity. Based on cluster and discriminant analysis we categorized astrocytes into two groups with respect to complexity, and designated



as type I the astrocytes that exhibited significantly higher values of complexity in comparison with type II.

Figure 6 and Tables 3 and 4 demonstrate the influences of age and environmental effects on the complexity of type I and II astrocytes (A–C) and on the “mean astrocyte” (D–F). In the last case complexity represents the mean of complexity of all astrocytes (without distinction

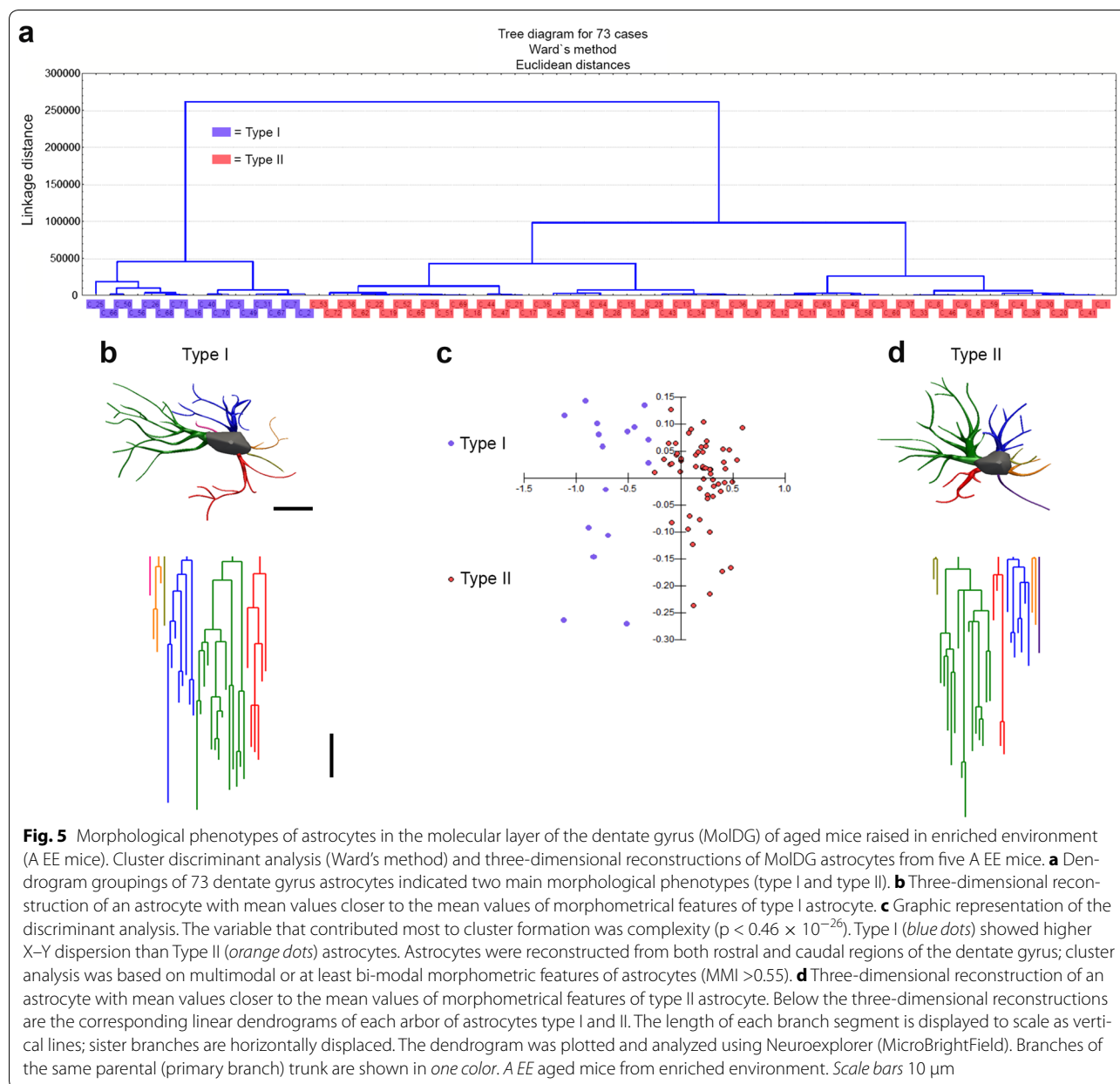
between type I and II). Two-way ANOVA applied to the “mean astrocyte” complexity values revealed that aging and environmental impoverishment, acting together, reduces astrocytes complexity (Table 3). However, the analysis of aging and environment influences on complexity of type I and II astrocytes separately (Fig. 6), revealed that the long term effects of aging and environment seems



to affect type I and type II astrocytes from aged mice raised in enriched environment to a greater extent than astrocytes from aged mice maintained in standard environment (Table 4). Indeed, in the molecular layer, except for the A-SE group, which was submitted to impoverishment environment throughout life, type I cells were preserved quite distinct from type II in terms of complexity in all groups. Type I astrocytes were more complex in young adults than in aged groups and more complex in aged mice raised in enriched environment than in

standard environment. However, type I astrocytes complexity mean values were not different from type II values in aged mice raised in standard environment.

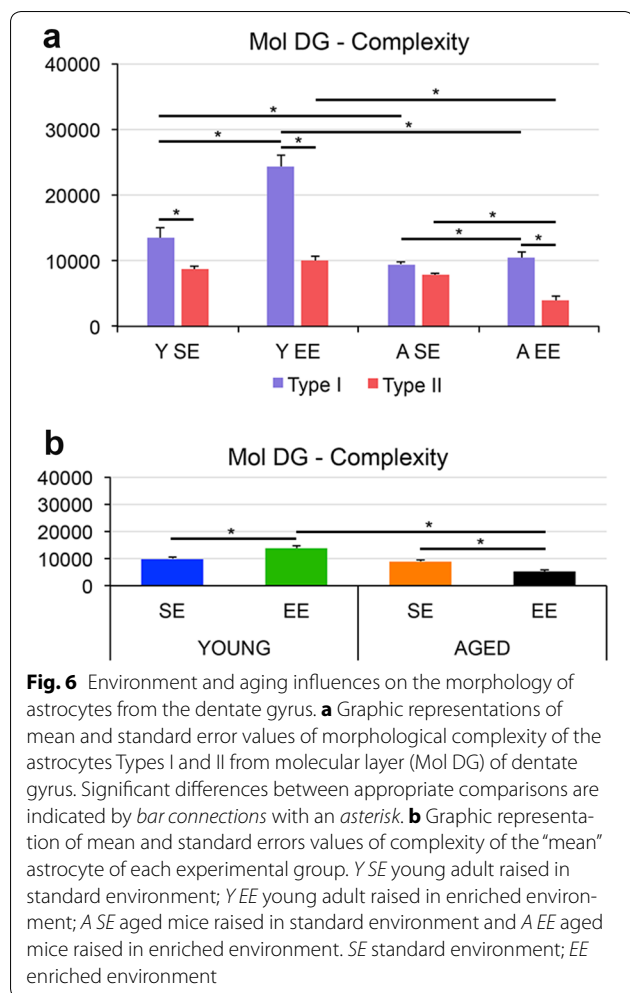
No simple correlations were detected between identity, placement or timing test results and the morphological complexity (Fig. 7). Similar analysis applied separately to type I or II astrocytes complexities and behavioral performances (not illustrated) showed similar negative results suggesting that cognition and morphological complexity of dentate gyrus astrocytes may not be linearly related.



### Discussion

We used stereological random and systematic sampling [66], combined with 3-D reconstruction of astrocytes to show that astrocyte morphological complexity is experience-dependent. We also demonstrated that young mice with more complex astrocyte structures showed, on average, better performance in object recognition tests. To our knowledge, there are no previous findings that result from applying an unbiased sample approach with 3-D microscopic reconstruction to the assessment of an astrocytes' morphological phenotype in the mouse dentate gyrus. This approach was chosen to guarantee

that all regions from the area of interest would have the same probability of inclusion in the (systematic and randomized) sample, and that fine anatomical details (from 3-D reconstructed astrocytes) could be quantified in all experimental groups using unbiased methods. From this sampling approach, associated with cluster and discriminant analysis of the morphometric features, we have found that, with the exception of the aged mice raised in the standard environment, which showed great homogeneity in the morphology of astrocytes, two main morphological phenotypes occupy the molecular layer of the dentate gyrus in adult and aged female albino Swiss mice.



We also discovered that relatively few morphological parameters are sufficient to distinguish the morphological changes in astrocytes associated with environment and age in our sample. Because complexity was the

morphological feature that best exemplifies such morphological changes, we will discuss it as a basis for the classification of astrocytes, as well as possible functional implications.

### Aging, astrocytes’ morphological complexity and object recognition

Emerging evidence indicates that the number of cells that express biomarkers of cellular senescence increases with aging and astrocytes in the aging brain express characteristics of senescence-associated secretory phenotype. Indeed, aged astrocytes exhibit increased intermediate GFAP- and vimentin-positive filaments, increased expression of several cytokines (TNF $\alpha$ , IL-1 $\beta$ , and IL-6) in the rat brain [67], and increased accumulation of proteotoxic aggregates [68]. Indeed, aged astrocytes exhibit increased intermediate GFAP- and vimentin-positive filaments, increased expression of several cytokines (TNF $\alpha$ , IL-1 $\beta$ , and IL-6) in the rat brain [67], and increased accumulation of proteotoxic aggregates [68]. However, the increase in GFAP-positive filaments in the aging brain is not a consensus. As reported elsewhere, changes in astroglia in ageing and neurodegeneration seem to be highly heterogeneous and region-specific [69] and this include significant differences between white and grey matter astrocytic and microglial activation as ageing progresses [70]. In addition, hippocampal astrocyte cultures from adult and aged rats seem to reproduce changes in glial functionality observed in the aging brain and this seem to include a reduction in GFAP expression that may reflect astroglial degeneration at early stages followed by an increase of GFAP at late stages [71]. Independent of the reasons associated to these contradictory findings an important question that remain to be investigated is how these changes affect astrocytic glutamate exocytosis at the entorhinal-to-dentate granular cells (perforant pathway), because through this mechanism, astrocytes

**Table 2** Discriminant analysis summary to indicate the morphological variables that most contribute to cluster formation of types I and II astrocytes from the molecular layer of dentate gyrus of each experimental group

	Wilks’	Partial	F-remove	p level	Toler.	1-Toler.
<i>Molecular layer</i>						
Y EE						
Complexity	0.449649	0.574029	53.429	0.0000000003	0.809881	0.19012
Convex hull volume ( $\mu\text{m}^3$ )	0.337713	0.764293	22.205	0.0000116304	0.826130	0.17387
Y SE						
Convex hull volume ( $\mu\text{m}^3$ )	0.550693	0.4469105	84.15575	0.00000000000016	0.952663	0.04734
A EE						
Complexity	0.9949113	0.2732307	194.1735	2.946224E <sup>-22</sup>	0.9189208	0.08108

Because astrocytes from the molecular layer of aged mice from standard environment (A SE) were morphologically quite homogeneous (very short Euclidian distances), data is not included here

Y EE young mice from enriched environment; Y SE young mice from standard environment; A EE aged mice from Y enriched environment

**Table 3 Influences of age and environment on the morphological complexity of the “mean astrocyte” from molecular layer of dentate gyrus**

Molecular layer of dentate gyrus	F	P		
Age	49.529	0.000		
Environment	0.091	0.763		
Age and environment	32.231	0.000		
Two-tail t test	<i>Y EE</i> × <i>Y SE</i>	<i>Y EE</i> × <i>A EE</i>	<i>Y SE</i> × <i>A SE</i>	<i>A EE</i> × <i>A SE</i>
t=	34,475	85,256	10,210	−53,432
p=	0.001	<0.0001	0.309	<0.0001

Two-way ANOVA with correspondent F and p values and two-tail t tests with correspondent t and p values

*Y EE* young mice from enriched environment; *Y SE* young mice from standard environment; *A EE* aged mice from enriched environment; *A SE* aged mice from standard environment

**Table 4 Influences of age and environment on the morphological complexity of Type I and Type II astrocytes from molecular layer of dentate gyrus (Mol-DG)**

Mol-DG type I × II	<i>Y SE</i>	<i>Y EE</i>	<i>A SE</i>	<i>A EE</i>
t=	30,689	82,001	−14,087	129,240
p=	0.003	<0.0001	0.1629	<0.0001
Type I	<i>Y EE</i> × <i>Y SE</i>	<i>Y EE</i> × <i>A EE</i>	<i>Y SE</i> × <i>A SE</i>	<i>A EE</i> × <i>A SE</i>
t=	45,419	82,187	32,042	27,412
p=	<0.0001	<0.0001	0.003	0.010
Type II	<i>Y EE</i> × <i>Y SE</i>	<i>Y EE</i> × <i>A EE</i>	<i>Y SE</i> × <i>A SE</i>	<i>A EE</i> × <i>A SE</i>
t=	15,521	101,537	−0.8054	−70,682
p=	0.1234	<0.0001	0.4224	<0.0001

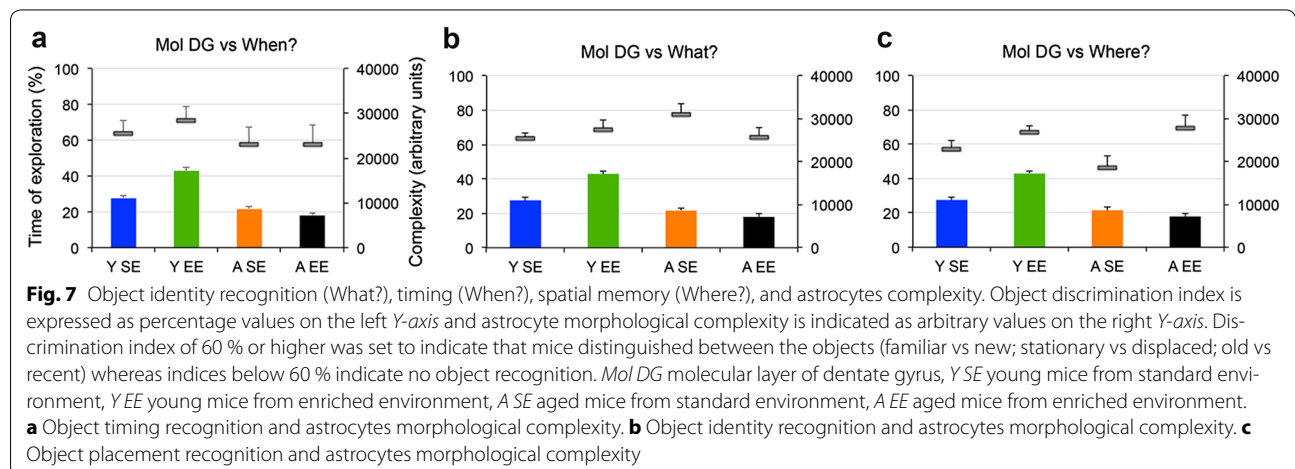
Two-tail t tests with correspondent t and p values

*Y EE* young mice from enriched environment; *Y SE* young mice from standard environment; *A EE* aged mice from enriched environment; *A SE* aged mice from standard environment

participate in synaptic tuning in circuits involved in cognitive processing and the control of mossy fiber-to-CA3 synaptic input [72]. In addition, even in the absence of

neurological disease, a more reactive astrocyte phenotype is expressed during aging as part of an increased and maintained pro-inflammatory profile that may be associated with cognitive dysfunction [73]. A decrease in the ability of aged rats to sustain long-term potentiation in the perforant pathway of the dentate gyrus also appears to be associated with microglial activation [74]. Taking these observations together, it would be reasonable to suggest that the number of astrocytes with senescence-associated secretory phenotype may be increased in animals raised in standard conditions (reducing astrocytic complexity) compared with aged mice housed in enriched conditions [74]. Although this was not the case of the “mean astrocyte” of the molecular layer from aged mice of enriched environment, when we analyzed type I and type II separately, type I astrocytes were significantly more complex than type II in this mice group. In contrast, only one morphological phenotype was found in aged mice raised in standard environment and this was morphologically similar to type II astrocytes.

Object recognition enables the unambiguous distinction between new and familiar objects; see [75, 76] for recent reviews. To cope with memory tasks, the brain must accentuate the differences between old and new experiences before coding occurs [25]. For that purpose, medial and lateral perforant pathways transmit spatial and non-spatial information to the dentate gyrus, which is necessary for recognizing object placement (Where?), identity (What?), and timing (When?). Lateral portions of the entorhinal cortex project to the caudal levels of the dentate gyrus and hippocampus, and medial portions of the entorhinal cortex project to the rostral levels [77, 78]. We have learned from earlier experiments that only 6 mo. adult and aged mice from the enriched environment were able to integrate object recognition into a spatial-temporal context [13]. Mice from standard environments were unable to make the appropriate distinctions. In the spatial memory component of episodic-like memory (Where?),



young and aged animals housed in enriched conditions spent significantly more time in the displaced than stationary objects. In the identity and temporal memory components (What? and When?), young and aged animals housed in enriched conditions spent significantly more time in the old than recent objects [13]. Coherently, subsequent analysis of the behavior of aged mice found similar results in tasks that engaged episodic-like memory [79, 80] and working and recognition memories [81]. In the present report using object identity recognition, similar results were found. Indeed, all experimental groups recognized the identity of the objects, only mice from enriched environment (both young and aged) succeeded in the placement task, only young mice both from standard and enriched environments succeeded in the timing task but only young mice from enriched environment distinguished the context where the objects were displaced.

#### **Enriched environment, neurogenesis, spatial memory improvement and glial cells**

Neuronal progenitor cells in the subgranular zone continuously proliferate, migrate into the granular cell layer and differentiate into granule cells [82]. These new neurons, which have been implicated in pattern separation [83], are continually generated in the dentate gyrus in the adult hippocampus [35, 84]. Molecular layer perforant path-associated cells contribute to feed-forward inhibition of these granular cells in the adult dentate gyrus [85] and the integrity of these projections seems to be essential to maintain granular dendritic arbors [86] and spatial learning and memory [87]. Medial and lateral perforant pathways transmit to dentate gyrus, spatial and non-spatial information that would be necessary to learn and recognize object placement (Where?), identity (What?) and timing (When?) [88]. The newborn neurons targeted by perforant pathway, seem to increase significantly in the dentate gyrus of rodents raised in an enriched environment, and this has been associated with spatial memory improvements [89, 90]. In line with these observations our findings demonstrated that spatial memory is influenced by both age and environment and that object recognition memory seems to be resistant to both normal aging and impoverished environment of standard cages.

During our previous stereological analysis of the dentate gyrus of aged mice raised in standard environment, we observed hyperplasia of astrocytes in the molecular layer compared with equivalent sections from young adults raised in the same conditions. Interestingly, aged mice from enriched but not from standard exhibited the ability to form integrated memories in the spatial-temporal context [13]. However, environment and aging affected the molecular layer of the dentate gyrus

in an additive way; thus, we speculated that astrocytosis induced by environmental enrichment might have a different functional role from that induced by aging [13]. Paradoxically, our preliminary morphometric analysis in the molecular layer of the dentate gyrus, using a random but not systematic sampling approach, [45] confirmed earlier descriptions in aged rats [44], that hippocampal astrocytes from aged mice, maintained in an enriched environment, were smaller than those from aged mice maintained in a standard environment. In the present report, we confirmed our preliminary report on the “mean astrocyte” molecular layer. However, hierarchical cluster and discriminant analysis revealed two different morphological phenotypes that had their morphologies distinctly influenced by environment and age.

Although the molecular basis of those changes remains to be investigated, it is important to discuss possible implications associated with the influences of aging and the environment on the morphology of astrocytes in the dentate gyrus.

#### **Possible physiological implications of an increase in astrocytic complexity**

It is interesting to discuss possible connections between the quantitative astrocyte morphological response and the cognitive protection observed after environmental enrichment. In the rodent brain, a single astrocyte is the third element of hundreds of thousands of synapses [91–93]. This ramified complex morphological substrate provides the structural basis for functional interactions with neurons, other glial cell processes, and blood vessels [94]. Studies of neuronal stimulation and astrocyte morphology have taught us that astrocytes react to neuronal stimulation by changing their morphology, and ultrastructural analysis of targeted projections from the stimulated region have demonstrated that neural stimulation causes a significant increase in the astrocytic envelopment of excitatory synapses on dendritic spines [95].

Our findings showed that mice living all life on an impoverished environment lose astrocytic morphological diversity. In contrast, individuals maintained for the same time extent in an enriched environment, did not lose astrocytic diversity. Indeed, 6 months of enriched environment increase 113 % the number of higher complexity astrocytes, and the absolute number of these type I astrocytes are not reduced later in life. Aged mice from enriched environment showed the same number of type I astrocytes. Although type II is less influenced by environmental changes (26 % increase in Y EE vs Y SE), it seems that this morphological phenotype is responsible for significant increase in the total number of astrocytes on aged mice from enriched environment (Fig. 8).

Because environmental enrichment is associated with a greater degree of long-term somatosensory/motor and visuospatial stimulation, and in the present report, we observed better performance of an object recognition placement and context tasks in young mice from the enriched environment, with more complex astrocytes, we suggest that at least part of this improvement in hippocampal-dependent tasks performances in young mice, might be associated with astrocytic plasticity. These findings are in line with recent report which demonstrate that housing complexity alters GFAP-immunoreactive astrocyte morphology in the rat dentate gyrus [41]. It is important to highlight that our analysis was done in the molecular layer of dentate gyrus, the main target of the perforant pathway and type I astrocytes were more ramified and longer than type II. Thus, it is reasonable to propose they will affect a higher number of synapses in that layer than type II.

Because type I morphology is affected in higher proportion by aging and environmental impoverishment than type II and aged mice raised in enriched environment had better performances in hippocampal-dependent tasks than aged mice from standard environment it is reasonable to propose different physiological roles for these two phenotypes.

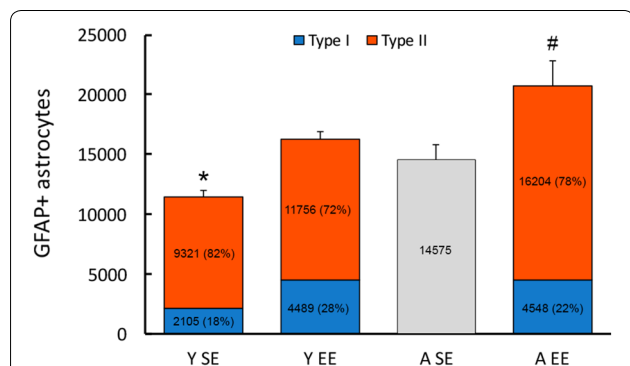


**Fig. 8** Environment and aging influences on the number and morphology of astrocytes from the molecular layer of dentate gyrus. Relative number of astrocytes morphological phenotypes Type I and Type II as a function of the total number of GFAP immunolabeled astrocytes (GFAP + astrocytes). To estimate these numbers, we used percentage values of type I and type II reconstructed astrocytes in combination with previous stereological data described elsewhere [106]. Note that young mice independent of environment, and aged mice from enriched environment show Type I and II morphological phenotypes, whereas aged mice from standard environment did not. *Y SE* young adult raised in standard environment; *Y EE* young adult raised in enriched environment; *A SE* aged mice raised in standard environment and *A EE* aged mice raised in enriched environment. *SE* standard environment; *EE* enriched environment. (\*) and (#) indicate significant differences between the number of total astrocytes from different experimental groups (Y EE vs Y SE; Y EE vs A EE; Y SE vs A SE; A EE vs A SE)

### Hormones and astrocytes

When male Swiss mice were group housed in the laboratory, aggressive interactions between cage mates caused severe injury and stress in the animals. These findings previously described elsewhere, may hamper the validity of experimental results, for review see [96]. To minimize the level of aggression in the cages, female mice were chosen to compose the experimental groups. This choice however, may have included estrogenic changes late in life induced by aging, that may contribute to age-related cognitive impairments and to associated astrocytic morphological changes. Indeed, apart from aging and environment, sexual hormones may change the number [97–99] and morphology [98, 100] of neuroglial cells. In the dentate gyrus, aged C57Bl6 female mice presented 35 % more astrocytes than age-matched males [97] and estrogen and raloxifene changed both the number and morphology of astrocytes of aged female mice [101]. In the present report, aged females may have been depleted of estrogenic protection; thus, we suggest that at least part of the morphological changes detected in aged female mice from both enriched and impoverished environments might be related to estropause. In agreement, ovariectomized female mice given an estrogenic replacement showed significant changes in both the number and morphology of astrocytes in the dentate gyrus compared to an ovariectomized placebo group [101].

Finally, it is important to consider that manipulation-induced stress during behavioral tasks might have altered plasma corticosteroid levels, with implications on astrocytic plasticity [102]. Although we cannot exclude the possibility that different levels of corticosteroids might explain the results the behavioral tests were applied to all animals of all experimental groups which minimizes the possibility that manipulation-induced stress might explain the results.

### Limitations of the experimental design and technical approaches

Comparative analysis of different astrocytes immunomarkers demonstrated that anti-GFAP immunolabeling offers complementary information to anti-S-100β or anti-glutamine synthetase [103]. Indeed, morphometric analysis of astrocytes, labeled with these three distinct markers revealed region-specific changes in the astroglial morphological phenotypes.

Although the number of GFAP immunolabeled astrocytes may not represent the total number of astrocytes, we and others using GFAP immunolabeling and unbiased stereological methods demonstrated that age [13, 97] and environmental changes [13] were associated with significant changes in the number of the subpopulation of GFAP immunolabeled astrocytes in dentate gyrus.

In addition, the environmental enrichment stimulated neurogenesis and gliogenesis [104], increased the GFAP immunolabeled cellular network [105], showing astrocytes with longer branches and higher number of branching points [43, 46]. We [45] and others [32, 44, 46, 103] also demonstrated that as compared to aged mice raised in standard environment, long-life environmental enrichment is associated with shorter GFAP astrocytes branches, lower number of nodes and reduction in the tree surface areas and complexity.

Finally, the influences of environmental enrichment and age on astrocytes' morphological changes and memory investigated previously in mice and rats using different approaches, models, and techniques [13, 43, 44, 105, 106] were sometimes contradictory. Because different methods, different animal lineages, variations in histological procedures, different stereological protocols, and ambiguities in the definition of the objects and areas of interest were applied, it is reasonable to suppose that at least part of these contradictions might be explained by these differences. To minimize possible sources of variations all samples were obtained with the same tissue processing protocols (perfusion, immunoreaction, dehydration, counterstaining, and clearing) and all data were collected and analyzed with the same unbiased methodology. We also confirmed the results by having different investigators reconstructing the same cells, using the same monoclonal anti-GFAP antibody as a selective marker for astrocytes. Thus, it is expected that non-biological sources were reduced to acceptable levels in the present report [97, 107]. Microscopic, 3-D reconstructions might be affected by non-uniform shrinkage in the z-axis of sections [108]. It was recently demonstrated that sections that the final thickness in the Z-axis is approximately 25 % of the cut thickness after dehydration and clearing [62]. We used this percentage value to implement corrections on all astrocyte reconstructions, assuming 75 % shrinkage of thickness along the z-axis and because the tissue size did not change along X–Y axes after histological dehydration and clearing no corrections were applied to the x/y dimensions.

## Conclusions

Using a combination of stereological sampling approach and three-dimensional reconstruction we found two morphological phenotypes on the molecular layer of dentate gyrus. On average, type I morphological complexity seems to be much more sensitive to age and environmental influences than that of type II. Indeed, aging and environmental impoverishment interact and reduce the morphological complexity of type I astrocytes at a point that they could not be distinguished anymore from type II. Our findings confirm previous reports that the morphological complexity of astrocytes is experience-dependent and suggest at least

in young mice that astrocytes of higher complexity may be associated with better performances in object recognition hippocampal-dependent tasks. Although aged mice from enriched environment preserved object recognition, their astrocytes revealed significant degree of shrinkage.

## Additional file

**Additional file 1: Table S1.** Object exploration time (s).

## Abbreviations

A EE: aged mice raised in enriched environment; Y EE: young mice raised in enriched environment; A SE: aged mice raised in standard environment; Y SE: young mice raised in standard environment; GFAP: glial fibrillary acid protein; GrDG: granular layer of the dentate gyrus; MolDG: molecular layer of the dentate gyrus; PolDG: polymorphic layer of the dentate gyrus; 3-D: three-dimensional.

## Authors' contributions

Study concept and design: CWPD, DGD, PFCV and JBT. Acquisition of data: CARF, MAO, CML, DGD. Analysis and interpretation of data: JBT, DCA, DGD, CWPD, MCKS. Drafting of the manuscript: CWPD, DCA, JBT and DGD. Critical revision of the manuscript for important intellectual content: DCA, CWPD, JBT, DGD. Statistical analysis: JBT, DGD, CWPD. Obtained funding: CWPD, PFCV. Administrative, technical and material support: CARF, MCKS, CML, MAO. Study supervision: CWPD. All authors read and approved the final manuscript.

## Author details

<sup>1</sup> Laboratório de Investigações Em Neurodegeneração e Infecção, Instituto de Ciências Biológicas, Universidade Federal do Pará, Hospital Universitário João de Barros Barreto, Rua dos Mundurucus 4487, Guamá, Belém, Pará CEP 66073-000, Brazil. <sup>2</sup> Departamento de Arbovirologia e Febres Hemorrágicas, Instituto Evandro Chagas, Ananindeua, Pará, Brazil. <sup>3</sup> Laboratory of Experimental Neuropathology, Department of Pharmacology, University of Oxford, Oxford, England, UK.

## Acknowledgements

Not applicable.

## Competing interests

The authors declare that they have no competing interests.

## Ethics approval

All procedures were approved by the institutional animal care committee of the Federal University of Pará. All animals were handled in accordance with the "Guidelines for the Use of Animals in Research" and followed the legal requirements of the Brazilian Council of Experimental Animal Research—CONCEA.

## Funding

This study received financial support from Conselho Nacional de Pesquisa—CNPq (Grant Numbers: 300203/2010-1, 471077/2007-0 and 441007/2014-7) for CWPD; Coordenação de Aperfeiçoamento de Pessoal de Nível Superior—CAPES (Process Number: 99999.001533/2014-02) for CWPD; Universidade Federal do Pará—Edital PROPESP/FADESP—PIAPA 2015.

Received: 23 June 2016 Accepted: 22 September 2016

Published online: 10 October 2016

## References

1. Tyndall AV, Davenport MH, Wilson BJ, Burek GM, Arseneault-Lapierre G, Haley E, Eskes GA, Friedenreich CM, Hill MD, Hogan DB, et al. The brain-in-motion study: effect of a 6-month aerobic exercise intervention on cerebrovascular regulation and cognitive function in older adults. *BMC Geriatr.* 2013;13:21.

2. Erickson KI, Weinstein AM, Lopez OL. Physical activity, brain plasticity, and Alzheimer's disease. *Arch Med Res*. 2012;43:615–21.
3. Small BJ, Dixon RA, McArdle JJ, Grimm KJ. Do changes in lifestyle engagement moderate cognitive decline in normal aging? Evidence from the Victoria Longitudinal Study. *Neuropsychology*. 2012;26:144–55.
4. Fernández-Mayoralas G, Rojo-Pérez F, Martínez-Martín P, Prieto-Flores ME, Rodríguez-Blázquez C, Martín-García S, Rojo-Abuín JM, Forjaz MJ. Active ageing and quality of life: factors associated with participation in leisure activities among institutionalized older adults, with and without dementia. *Aging Ment Health*. 2015;19:1031–41.
5. Pedrero-Chamizo R, Albers U, Tobaruela JL, Meléndez A, Castillo MJ, González-Gross M. Physical strength is associated with Mini-Mental State Examination scores in Spanish institutionalized elderly. *Geriatr Gerontol Int*. 2013;13:1026–34.
6. Lovden M, Xu W, Wang HX. Lifestyle change and the prevention of cognitive decline and dementia: what is the evidence? *Curr Opin Psychiatry*. 2013;26:239–43.
7. Zhao E, Tranovich MJ, Wright VJ. The role of mobility as a protective factor of cognitive functioning in aging adults: a review. *Sports Health*. 2014;6:63–9.
8. Stranahan AM, Mattson MP. Metabolic reserve as a determinant of cognitive aging. *J Alzheimers Dis*. 2012;30(Suppl 2):S5–13.
9. Mangialasche F, Kivipelto M, Solomon A, Fratiglioni L. Dementia prevention: current epidemiological evidence and future perspective. *Alzheimers Res Ther*. 2012;4:6.
10. Volkens KM, Scherder EJ. Impoverished environment, cognition, aging and dementia. *Rev Neurosci*. 2011;22:259–66.
11. Zalik E, Zalar B. Differences in mood between elderly persons living in different residential environments in Slovenia. *Psychiatr Danub*. 2013;25:40–8.
12. Maseda A, Balo A, Lorenzo-López L, Lodeiro-Fernández L, Rodríguez-Villamil JL, Millán-Calenti JC. Cognitive and affective assessment in day care versus institutionalized elderly patients: a 1-year longitudinal study. *Clin Interv Aging*. 2014;9:887–94.
13. Diniz D, Foro CA, Rego C, Gloria DA, de Oliveira FR, Paes JM, de Sousa AA, Tokuhashi TP, Trindade LS, Turiel MC, et al. Environmental impoverishment and aging alter object recognition, spatial learning, and dentate gyrus astrocytes. *Eur J Neurosci*. 2010;32:509–19.
14. Teather LA, Wurtman RJ. Chronic administration of UMP ameliorates the impairment of hippocampal-dependent memory in impoverished rats. *J Nutr*. 2006;136:2834–7.
15. Teather LA, Wurtman RJ. Dietary CDP-choline supplementation prevents memory impairment caused by impoverished environmental conditions in rats. *Learn Mem*. 2005;12:39–43.
16. Gregory ML, Szumlinski KK. Impoverished rearing impairs working memory and metabotropic glutamate receptor 5 expression. *NeuroReport*. 2008;19:239–43.
17. Mendes Fde C, de Almeida MN, Felício AP, Fadel AC, Silva Dde J, Borralho TG, da Silva RP, Bento-Torres J, Vasconcelos PF, Perry VH, et al. Enriched environment and masticatory activity rehabilitation recover spatial memory decline in aged mice. *BMC Neurosci*. 2013;14:63.
18. Winocur G. Environmental influences on cognitive decline in aged rats. *Neurobiol Aging*. 1998;19:589–97.
19. Bell JA, Livesey PJ, Meyer JF. Environmental enrichment influences survival rate and enhances exploration and learning but produces variable responses to the radial maze in old rats. *Dev Psychobiol*. 2009;51:564–78.
20. Kumar A, Rani A, Tchigranova O, Lee WH, Foster TC. Influence of late-life exposure to environmental enrichment or exercise on hippocampal function and CA1 senescent physiology. *Neurobiol Aging*. 2012;33:828 (e821–817).
21. Speisman RB, Kumar A, Rani A, Pastoriza JM, Severance JE, Foster TC, Ormerod BK. Environmental enrichment restores neurogenesis and rapid acquisition in aged rats. *Neurobiol Aging*. 2012;34:263–74.
22. Speisman RB, Kumar A, Rani A, Pastoriza JM, Severance JE, Foster TC, Ormerod BK. Environmental enrichment restores neurogenesis and rapid acquisition in aged rats. *Neurobiol Aging*. 2013;34:263–74.
23. Speisman RB, Kumar A, Rani A, Foster TC, Ormerod BK. Daily exercise improves memory, stimulates hippocampal neurogenesis and modulates immune and neuroimmune cytokines in aging rats. *Brain Behav Immun*. 2013;28:25–43.
24. Yuan Z, Wang M, Yan B, Gu P, Jiang X, Yang X, Cui D. An enriched environment improves cognitive performance in mice from the senescence-accelerated prone mouse 8 strain: role of upregulated neurotrophic factor expression in the hippocampus. *Neural Regen Res*. 2012;7:1797–804.
25. Schmidt B, Marrone DF, Markus EJ. Disambiguating the similar: the dentate gyrus and pattern separation. *Behav Brain Res*. 2012;226:56–65.
26. Cheng L, Wang SH, Jia N, Xie M, Liao XM. Environmental stimulation influence the cognition of developing mice by inducing changes in oxidative and apoptosis status. *Brain Dev*. 2014;36:51–6.
27. Leger M, Quiedeville A, Paizanis E, Natkunarajah S, Freret T, Boulouard M, Schumann-Bard P. Environmental enrichment enhances episodic-like memory in association with a modified neuronal activation profile in adult mice. *PLoS One*. 2012;7:e48043.
28. Suzuki H, Kanagawa D, Nakazawa H, Tawara-Hirata Y, Kogure Y, Shimizu-Okabe C, Takayama C, Ishikawa Y, Shiosaka S. Role of neuropsin in parvalbumin immunoreactivity changes in hippocampal basket terminals of mice reared in various environments. *Front Cell Neurosci*. 2014;8:420.
29. Bureš Z, Bartošová J, Lindovský J, Chumak T, Popelář J, Syka J. Acoustical enrichment during early postnatal development changes response properties of inferior colliculus neurons in rats. *Eur J Neurosci*. 2014;40:3674–83.
30. Vallès A, Granic I, De Weerd P, Martens GJ. Molecular correlates of cortical network modulation by long-term sensory experience in the adult rat barrel cortex. *Learn Mem*. 2014;21:305–10.
31. Hosseiny S, Pietri M, Petitpaitel A, Zarif H, Heurteaux C, Chabry J, Guyon A. Differential neuronal plasticity in mouse hippocampus associated with various periods of enriched environment during postnatal development. *Brain Struct Funct*. 2014;220:3435–48.
32. Sampedro-Piquero P, Begega A, Arias JL. Increase of glucocorticoid receptor expression after environmental enrichment: relations to spatial memory, exploration and anxiety-related behaviors. *Physiol Behav*. 2014;129:118–29.
33. Kobilto T, Liu QR, Gandhi K, Mughal M, Shaham Y, van Praag H. Running is the neurogenic and neurotrophic stimulus in environmental enrichment. *Learn Mem*. 2011;18:605–9.
34. van Praag H, Shubert T, Zhao C, Gage FH. Exercise enhances learning and hippocampal neurogenesis in aged mice. *J Neurosci*. 2005;25:8680–5.
35. Kempermann G, Kuhn HG, Gage FH. More hippocampal neurons in adult mice living in an enriched environment. *Nature*. 1997;386:493–5.
36. Ramírez-Rodríguez G, Ocaña-Fernández MA, Vega-Rivera NM, Torres-Pérez OM, Gómez-Sánchez A, Estrada-Camarena E, Ortiz-López L. Environmental enrichment induces neuroplastic changes in middle age female Balb/c mice and increases the hippocampal levels of BDNF, p-Akt and p-MAPK1/2. *Neuroscience*. 2014;260:158–70.
37. Merkley CM, Jian C, Mosa A, Tan YF, Wojtowicz JM. Homeostatic regulation of adult hippocampal neurogenesis in aging rats: long-term effects of early exercise. *Front Neurosci*. 2014;8:174.
38. Bergami M, Masserdotti G, Temprana SG, Motori E, Eriksson TM, Göbel J, Yang SM, Conzelmann KK, Schinder AF, Götz M, Berninger B. A critical period for experience-dependent remodeling of adult-born neuron connectivity. *Neuron*. 2015;85:710–7.
39. Donato F, Chowdhury A, Lahr M, Caroni P. Early- and late-born parvalbumin basket cell subpopulations exhibiting distinct regulation and roles in learning. *Neuron*. 2015;85:770–86.
40. Huang W, Ming GL, Song H. Experience matters: enrichment remodels synaptic inputs to adult-born neurons. *Neuron*. 2015;85:659–61.
41. Salois G, Smith JS. Housing complexity alters GFAP-immunoreactive astrocyte morphology in the rat dentate gyrus. *Neural Plast*. 2016;2016:3928726.
42. Zorec R, Horvat A, Vardjan N, Verkhatsky A. Memory Formation Shaped by Astroglia. *Front Integr Neurosci*. 2015;9:56. doi:10.3389/fnint.2015.00056.
43. Sampedro-Piquero P, De Bartolo P, Petrosini L, Zancada-Menendez C, Arias JL, Begega A. Astrocytic plasticity as a possible mediator of the cognitive improvements after environmental enrichment in aged rats. *Neurobiol Learn Mem*. 2014;114:16–25.

44. Soffie M, Hahn K, Terao E, Eclancher F. Behavioural and glial changes in old rats following environmental enrichment. *Behav Brain Res*. 1999;101:37–49.
45. Diniz D, Foro C, Bento-Torres J, Vasconcelos P, Diniz CW. Aging, environmental enrichment, object recognition and astrocyte plasticity in dentate gyrus. In: Gonzalez-Perez O, editor. *Astrocytes: structure, functions and role in disease*. 1st ed. Hauppauge, New York: Nova Science Publisher Inc; 2012. p. 91–108.
46. Viola GG, Rodrigues L, Americo JC, Hansel G, Vargas RS, Biasibetti R, Swarowsky A, Goncalves CA, Xavier LL, Achaval M, et al. Morphological changes in hippocampal astrocytes induced by environmental enrichment in mice. *Brain Res*. 2009;1274:47–54.
47. Han X, Chen M, Wang F, Windrem M, Wang S, Shanz S, Xu Q, Oberheim NA, Bekar L, Betstadt S, et al. Forebrain engraftment by human glial progenitor cells enhances synaptic plasticity and learning in adult mice. *Cell Stem Cell*. 2013;12:342–53.
48. Windrem MS, Schanz SJ, Guo M, Tian GF, Washco V, Stanwood N, Rasband M, Roy NS, Nedergaard M, Havton LA, et al. Neonatal chimerization with human glial progenitor cells can both remyelinate and rescue the otherwise lethally hypomyelinated shiverer mouse. *Cell Stem Cell*. 2008;2:553–65.
49. Zhang Y, Barres BA. A smarter mouse with human astrocytes. *Bioessays*. 2013;35:876–80.
50. Franklin RJ, Bussey TJ. Do your glial cells make you clever? *Cell Stem Cell*. 2013;12:265–6.
51. Oberheim NA, Wang X, Goldman S, Nedergaard M. Astrocytic complexity distinguishes the human brain. *Trends Neurosci*. 2006;29:547–53.
52. Oberheim NA, Takano T, Han X, He W, Lin JH, Wang F, Xu Q, Wyatt JD, Pilcher W, Ojemann JG, et al. Uniquely hominid features of adult human astrocytes. *J Neurosci*. 2009;29:3276–87.
53. Witter MP. The perforant path: projections from the entorhinal cortex to the dentate gyrus. *Prog Brain Res*. 2007;163:43–61.
54. Smith AC, Frank LM, Wirth S, Yanike M, Hu D, Kubota Y, Graybiel AM, Suzuki WA, Brown EN. Dynamic analysis of learning in behavioral experiments. *J Neurosci*. 2004;24:447–61.
55. Dere E, Huston JP, De Souza Silva MA. Episodic-like memory in mice: simultaneous assessment of object, place and temporal order memory. *Brain Res Brain Res Protoc*. 2005;16:10–9.
56. Dere E, Huston JP, De Souza Silva MA. Integrated memory for objects, places, and temporal order: evidence for episodic-like memory in mice. *Neurobiol Learn Mem*. 2005;84:214–21.
57. Dere E, Huston JP, De Souza Silva MA. The pharmacology, neuroanatomy and neurogenetics of one-trial object recognition in rodents. *Neurosci Biobehav Rev*. 2007;31:673–704.
58. Tulving E. Episodic memory and common sense: how far apart? *Philos Trans R Soc Lond B Biol Sci*. 2001;356:1505–15.
59. Dix SL, Aggleton JP. Extending the spontaneous preference test of recognition: evidence of object-location and object-context recognition. *Behav Brain Res*. 1999;99:191–200.
60. Dere M, Huston JP, Silva MAS. Episodic-like memory in mice: simultaneous assessment of object, place and temporal order memory. *Brain Res*. 2005;16:10–9.
61. Shu S, Ju G, Fan L. The glucose oxidase-DAB-nickel method in peroxidase histochemistry of the nervous system. *Neurosci Lett*. 1988;85:169–71.
62. Carlo CN, Stevens CF. Analysis of differential shrinkage in frozen brain sections and its implications for the use of guard zones in stereology. *J Comp Neurol*. 2011;519:2803–10.
63. Schweitzer L, Renehan WE. The use of cluster analysis for cell typing. *Brain Res Brain Res Protoc*. 1997;1:100–8.
64. Kolb H, Fernandez E, Schouten J, Ahnelt P, Linberg KA, Fisher SK. Are there three types of horizontal cell in the human retina? *J Comp Neurol*. 1994;343:370–86.
65. Pillai AG, de Jong D, Kanatsou S, Krugers H, Knapman A, Heinzmann JM, Holsboer F, Landgraf R, Joëls M, Touma C. Dendritic morphology of hippocampal and amygdalar neurons in adolescent mice is resilient to genetic differences in stress reactivity. *PLoS One*. 2012;7:e38971.
66. West MJ. Stereological methods for estimating the total number of neurons and synapses: issues of precision and bias. *Trends Neurosci*. 1999;22(2):51–61.
67. Campuzano O, Castillo-Ruiz MM, Acarin L, Castellano B, Gonzalez B. Increased levels of proinflammatory cytokines in the aged rat brain attenuate injury-induced cytokine response after excitotoxic damage. *J Neurosci Res*. 2009;87:2484–97.
68. Salminen A, Ojala J, Kaarniranta K, Haapasalo A, Hiltunen M, Soininen H. Astrocytes in the aging brain express characteristics of senescence-associated secretory phenotype. *Eur J Neurosci*. 2011;34:3–11.
69. Rodríguez-Arellano JJ, Párpura V, Zorec R, Verkhatsky A. Astrocytes in physiological aging and Alzheimer's disease. *Neuroscience*. 2016;323:170–82.
70. Robillard KN, Lee KM, Chiu KB, MacLean AG. Glial cell morphological and density changes through the lifespan of rhesus macaques. *Brain Behav Immun*. 2016;55:60–9.
71. Bellaver B, Souza DG, Souza DO, Quincozes-Santos A. Hippocampal astrocyte cultures from adult and aged rats reproduce changes in glial functionality observed in the aging brain. *Mol Neurobiol*. 2016:1–17. doi:10.1007/s12035-016-9880-8.
72. Jourdain P, Bergersen LH, Bhaukaurally K, Bezzi P, Santello M, Domercq M, Matute C, Tonello F, Gundersen V, Volterra A. Glutamate exocytosis from astrocytes controls synaptic strength. *Nat Neurosci*. 2007;10:331–9.
73. Godbout JP, Johnson RW. Age and neuroinflammation: a lifetime of psychoneuroimmune consequences. *Immunol Allerg Clin North Am*. 2009;29:321–37.
74. Lynch MA. Age-related neuroinflammatory changes negatively impact on neuronal function. *Front Aging Neurosci*. 2010;1:6.
75. Pause BM, Zlomuzica A, Kinugawa K, Mariani J, Pietrowsky R, Dere E. Perspectives on episodic-like and episodic memory. *Front Behav Neurosci*. 2013;7:33.
76. Eichenbaum H, Sauvage M, Fortin N, Komorowski R, Lipton P. Towards a functional organization of episodic memory in the medial temporal lobe. *Neurosci Biobehav Rev*. 2012;36:1597–608.
77. Witter MP, Van Hoesen GW, Amaral DG. Topographical organization of the entorhinal projection to the dentate gyrus of the monkey. *J Neurosci*. 1989;9(1):216–28.
78. Witter MP, Amaral DG. Entorhinal cortex of the monkey: V. Projections to the dentate gyrus, hippocampus, and subicular complex. *J Comp Neurol*. 1991;307(3):437–59.
79. Davis KE, Eacott MJ, Easton A, Gigg J. Episodic-like memory is sensitive to both Alzheimer's-like pathological accumulation and normal ageing processes in mice. *Behav Brain Res*. 2013;254:73–82.
80. Tronche C, Lestage P, Louis C, Carrie I, Béracochéa D. Pharmacological modulation of contextual "episodic-like" memory in aged mice. *Behav Brain Res*. 2010;215:255–60.
81. Da Silva Costa-Aze V, Dauphin F, Boulouard M. Serotonin 5-HT6 receptor blockade reverses the age-related deficits of recognition memory and working memory in mice. *Behav Brain Res*. 2011;222:134–40.
82. Cameron HA, Woolley CS, McEwen BS, Gould E. Differentiation of newly born neurons and glia in the dentate gyrus of the adult rat. *Neuroscience*. 1993;56:337–44.
83. Nakashiba T, Cushman JD, Pelkey KA, Renaudineau S, Buhl DL, McHugh TJ, Rodriguez Barrera V, Chittajallu R, Iwamoto KS, McBain CJ, et al. Young dentate granule cells mediate pattern separation, whereas old granule cells facilitate pattern completion. *Cell*. 2012;149:188–201.
84. Zhao C, Deng W, Gage FH. Mechanisms and functional implications of adult neurogenesis. *Cell*. 2008;132:645–60.
85. Li Y, Stam FJ, Aimone JB, Goulding M, Callaway EM, Gage FH. Molecular layer perforant path-associated cells contribute to feed-forward inhibition in the adult dentate gyrus. *Proc Natl Acad Sci USA*. 2013;110:9106–11.
86. Vuksic M, Del Turco D, Vlachos A, Schuldt G, Müller CM, Schneider G, Deller T. Unilateral entorhinal denervation leads to long-lasting dendritic alterations of mouse hippocampal granule cells. *Exp Neurol*. 2011;230:176–85.
87. Moorthi P, Premkumar P, Priyanka R, Jayachandran KS, Anusuyadevi M. Pathological changes in hippocampal neuronal circuits underlie age-associated neurodegeneration and memory loss: positive clue toward SAD. *Neuroscience*. 2015;301:90–105.
88. Kesner RP, Rolls ET. A computational theory of hippocampal function, and tests of the theory: new developments. *Neurosci Biobehav Rev*. 2015;48:92–147.

89. Nilsson M, Perfilieva E, Johansson U, Orwar O, Eriksson PS. Enriched environment increases neurogenesis in the adult rat dentate gyrus and improves spatial memory. *J Neurobiol*. 1999;39:569–78.
90. Bruel-Jungerman E, Laroche S, Rampon C. New neurons in the dentate gyrus are involved in the expression of enhanced long-term memory following environmental enrichment. *Eur J Neurosci*. 2005;21:513–21.
91. Halassa MM, Haydon PG. Integrated brain circuits: astrocytic networks modulate neuronal activity and behavior. *Annu Rev Physiol*. 2010;72:335–55.
92. Halassa MM, Fellin T, Haydon PG. Tripartite synapses: roles for astrocytic purines in the control of synaptic physiology and behavior. *Neuropharmacology*. 2009;57:343–6.
93. Halassa MM, Fellin T, Takano H, Dong JH, Haydon PG. Synaptic islands defined by the territory of a single astrocyte. *J Neurosci*. 2007;27:6473–7.
94. Reichenbach A, Derouiche A, Kirchhoff F. Morphology and dynamics of perisynaptic glia. *Brain Res Rev*. 2010;63:11–25.
95. Genoud C, Quairiaux C, Steiner P, Hirling H, Welker E, Knott GW. Plasticity of astrocytic coverage and glutamate transporter expression in adult mouse cortex. *PLoS Biol*. 2006;4:e343.
96. Van Loo PL, Van Zutphen LF, Baumans V. Male management: Coping with aggression problems in male laboratory mice. *Lab Anim*. 2003;37(4):300–13.
97. Mouton PR, Long JM, Lei DL, Howard V, Jucker M, Calhoun ME, Ingram DK. Age and gender effects on microglia and astrocyte numbers in brains of mice. *Brain Res*. 2002;956:30–5.
98. Johnson RT, Breedlove SM, Jordan CL. Sex differences and laterality in astrocyte number and complexity in the adult rat medial amygdala. *J Comp Neurol*. 2008;511:599–609.
99. Luquin S, Naftolin F, Garcia-Segura LM. Natural fluctuation and gonadal hormone regulation of astrocyte immunoreactivity in dentate gyrus. *J Neurobiol*. 1993;24:913–24.
100. Johnson RT, Schneider A, DonCarlos LL, Breedlove SM, Jordan CL. Astrocytes in the rat medial amygdala are responsive to adult androgens. *J Comp Neurol*. 2012;520:2531–44.
101. Lei DL, Long JM, Hengemihle J, O'Neill J, Manaye KF, Ingram DK, Mouton PR. Effects of estrogen and raloxifene on neuroglia number and morphology in the hippocampus of aged female mice. *Neuroscience*. 2003;121:659–66.
102. Liu WL, Lee YH, Tsai SY, Hsu CY, Sun YY, Yang LY, Tsai SH, Yang WC. Methylprednisolone inhibits the expression of glial fibrillary acidic protein and chondroitin sulfate proteoglycans in reactivated astrocytes. *Glia*. 2008;56:1390–400.
103. Rodríguez JJ, Yeh CY, Terzieva S, Olabarria M, Kulijewicz-Nawrot M, Verkhratsky A. Complex and region-specific changes in astroglial markers in the aging brain. *Neurobiol Aging*. 2014;35:15–23. doi:10.1016/j.neurobiolaging.2013.07.002.
104. van Praag H, Kempermann G, Gage FH. Running increases cell proliferation and neurogenesis in the adult mouse dentate gyrus. *Nat Neurosci*. 1999;2:266–70.
105. Williamson LL, Chao A, Bilbo SD. Environmental enrichment alters glial antigen expression and neuroimmune function in the adult rat hippocampus. *Brain Behav Immun*. 2012;26:500–10.
106. Diniz DG, Foro CAR, Rego CMD, Gloria DA, de Oliveira FRR, Paes JMP, de Sousa AA, Tokuhashi TP, Trindade LS, Turiel MCP, et al. Environmental impoverishment and aging alter object recognition, spatial learning, and dentate gyrus astrocytes. *Eur J Neurosci*. 2010;32:509–19.
107. Slomianka L, West MJ. Estimators of the precision of stereological estimates: an example based on the CA1 pyramidal cell layer of rats. *Neuroscience*. 2005;136(3):757–67.
108. Hosseini-Sharifabad M, Nyengaard JR. Design-based estimation of neuronal number and individual neuronal volume in the rat hippocampus. *J Neurosci Methods*. 2007;162:206–14.

Submit your next manuscript to BioMed Central and we will help you at every step:

- We accept pre-submission inquiries
- Our selector tool helps you to find the most relevant journal
- We provide round the clock customer support
- Convenient online submission
- Thorough peer review
- Inclusion in PubMed and all major indexing services
- Maximum visibility for your research

Submit your manuscript at  
[www.biomedcentral.com/submit](http://www.biomedcentral.com/submit)

